Soft Matter

Soft Matter

www.rsc.org/softmatter

ROYAL SOCIETY OF CHEMISTRY

Journal Name

ARTICLE

Magnetic microgels, a promising candidate for enhanced magnetic adsorbent particles in bioseparation: synthesis, physico-chemical characterization and separation performance

Rodica Turcu[*a], Vlad Socoliuc[*b], Izabell Craciunescu[a], Anca Petran[a], Anja Paulus[c], Matthias Franzreb[c], Eugeniu Vasile[d] and Ladislau Vekas[*b]

Abstract: For specific applications in the field of high gradient magnetic separation of biomaterials, magnetic nanoparticle clusters of controlled size and high magnetic moment in an external magnetic field are of particular interest. We report the synthesis and characterization of magnetic microgels designed for magnetic separation purposes, as well as the separation efficiency of the obtained microgel particles. High magnetization magnetic microgels with superparamagnetic behaviour have been obtained in a two-step synthesis procedure by miniemulsion technique using highly stable ferrofluid on volatile nonpolar carrier. Spherical clusters of closely packed hydrophobic oleic acid coated magnetite nanoparticles were coated with cross linked polymer shells of polyacrylic acid, poly-N-isopropylacrylamide, poly-3 - acrylamidopropyl trimethylammonium chloride. The morphology, size distribution, chemical surface composition and magnetic properties of the magnetic microgels were determined using transmission electron microscopy, X-ray Photoelectron Spectroscopy and vibrating sample magnetometer. Magnetically induced phase condensation in aqueous suspensions of magnetic microgels was investigated by optical microscopy and static light scattering. The condensed phase consists of elongated oblong structures oriented in the direction of the external magnetic field and may grow up to several microns thickness and tens or even hundreds of microns length. The dependence of phase condensation magnetic supersaturation on the magnetic field intensity was determined. The experiments using High Gradient Magnetic Separator show high values of the separation efficiency (99.9 – 99.97%) for the magnetic microgels.

1. Introduction

Polymer-magnetic nanoparticle hybrid materials offer a wide range of applications in the fields of biomedicine and biotechnology, e.g. in therapeutics, for multimodal imaging, targeted drug delivery, hyperthermia, analyte monitoring and recovery, magnetic cell labelling, as well as enzyme and protein separations [1-5]. A wide variety of synthesis procedures have been reported which exploit the specific composition and property of both, the polymeric material and the magnetic nanoparticles used as primary materials, to achieve the required functionalization, morphology and magnetic nanoparticle volume distribution in various types of magnetic beads. The pioneering works of Mosbach et al [6, 7] and Ugelstad et al [8] already pointed out the outstanding features and high application potential for biotechnology and biomedicine of magnetoresponsive polymeric nanocomposites, as a result of

joining ferrofluid technology and advanced polymer chemistry. Large scale synthesis of superparamagnetic nanocomposite polymer microparticles with highly selective surface functionalities is a key issue of a realistic strategy for industrial separation of biomolecules, especially of proteins [5, 9, 10]. Among the advantages of the use of such particles in biotechnology are rapid binding and elution kinetics, even in the case of crude solutions containing e.g. cell debris, and the perspective of the use of efficient and cost-effective magnetic separators able to treat large feed volumes and to isolate high-value bioproducts from them [11]. With a magnetic purification strategy, usually involving high gradient magnetic fishing (HGMF) [9], it becomes possible to magnetically separate selected target biomolecules directly out of crude biological process liquors, such as fermentation broths, cell disruptates, plasma, milk, whey and plant extracts [10], avoiding sample pre-treatment stages, such as centrifugation, filtration and

membrane separation. A comprehensive review of very recent results on selective bioseparation by magnetic particles [12] evidences the progress in the field, in particular the development of scalable functionalized magnetic particle manufacturing technologies to be used in industrial scale magnetic bioseparation equipments. Among the most important issues to be addressed for further improvement of large scale processing technologies is the cost-effective synthesis of recyclable functionalized beads with high magnetic moment density for selective separation of high-value and high-concentration bioproducts.

For specific applications in the field of high gradient magnetic separation of biomaterials, magnetic nanoparticle clusters of controlled shape, size and high magnetic moment in an external magnetic field are of particular interest [13-16]. Provided with specific functional groups, the high surface area and high magnetic mobility of magnetic sorbents facilitate the achievement of the required binding capacity for various bioproducts and their rapid extraction from solution. The overall magnetic moment and magnetic behaviour of polymer microparticles is strongly dependent on the size and surface coating of enclosed magnetic nanoparticles, as well as on their localization either in the core, distributed over the volume or at the surface of the polymer bead [15]. To achieve a high resultant magnetic moment of microparticles in an applied magnetic field, the magnetic core / polymer shell structure is the most advantageous [14, 15, 17]. In the ideal case, densely packed clusters of surface coated superparamagnetic nanoparticles of 5-20 nm size form the core of polymeric magnetic microparticles. In the absence of an external magnetic field the resultant magnetic moment of the microparticles is zero, while in non-zero field the permanent magnetic moments of the nanoparticles align along the field direction resulting in a net magnetic moment of the particles. Efficient screening of dipole-dipole interactions between the constituent magnetic nanoparticles ensures the reversible nature of the magnetization process; after removing the external magnetic field the permanent magnetic moments of individual nanoparticles regain their random orientation due to thermal energy and the microparticles will possess negligible magnetic moment (no remanence). This switchable nature of the resultant magnetic moment is a key property of magnetic beads designed for magnetic separation purposes.

Concerning the preparation of the magnetic core-polymeric shell type particles the ferrofluid based techniques involve, among others, controlled clusterization of surface coated magnetic nanoparticles (MNPs) using an oil-in-water miniemulsion method [14-21]. The saturation magnetization of these colloidal clusters is dependent on the mean size of the MNPs, packing density and organic (non-magnetic) content and attains large values, e.g. 24.8 emu/g [13], 57 emu/g [20], ~60 emu/g [17] and 75.8 emu/g [22]. High separation efficiency for biomolecules within a HGMF process requires both, high magnetic moment and high surface area of the used beads. Higher surface area may be achieved by reducing the diameter of spherical particles, however this will reduce also the volume of the magnetic core and consequently, the magnetic mobility of the particles. The controlled clusterization of MNPs from ferrofluids allows adapting of the overall size and magnetic moment of microgel particles to the requirements of the separation device used.

In this paper we focus on magnetic microgels prepared in a two-step synthesis procedure using advanced ferrofluid manufacturing procedure and oil-in-water miniemulsion technique [17, 23]. In a first step, magnetic core particles are obtained by assembling hydrophobic, oleic acid coated Fe_3O_4 nanoparticles into water-dispersible nanoparticle clusters (NPC) by selective evaporation of the organic phase. In the second step, the high magnetization NPCs are coated with cross linked polymer shells having functional groups with cation exchange (CEX) or anion exchange (AEX) properties. The size, chemical surface composition and magnetic properties of the resulting NPCs and magnetic microgels were determined using transmission electron microscopy (TEM), X-ray photoelectron spectroscopy (XPS) and vibrating sample magnetometry (VSM). The influence of the external magnetic field on the magnetically induced phase condensation in aqueous suspensions of magnetic microgels is presented. The experiments using a High Gradient Magnetic Separator (HGMS) show that magnetic microgels are suitable for applications in magnetic separation.

2. Experimental

Materials

Sodium lauryl sulfate (SLS), Cetyl trimethyl ammonium bromide (CTAB), *N*-isopropylacrylamide (NIPA), Acrylic acid (AAc), *N*,*N*′-Methylenebis(acrylamide) (BIS), 3-acrylamidopropyl trimethylammonium chloride (APTAC), Ammonium persulfate (APS) were obtained from Sigma-Aldrich and used as received. Ferrofluid (FF) containing oleic acid (OA) monolayer-coated magnetite nanoparticles stably dispersed in a light hydrocarbon carrier (toluene), synthesized according to the procedure described in [24], was used for the preparation of magnetic nanoparticle clusters.

Preparation of magnetic nanoparticle clusters

According to the procedure described in [24], hydrophobic magnetite nanoparticles (Fe_3O_4.OA) were synthesized by chemical co-precipitation (at t ≈ 80ºC) of magnetite from an aqueous solutions of Fe^{3+} and Fe^{2+} ions in the presence of concentrated NH_4OH solution (25%), under atmospheric conditions. The chemisorbed OA coated MNPs were dispersed first in kerosene, followed by repeated flocculation-redispersion of surfaced MNPs in order to eliminate the excess (not chemisorbed) oleic acid. The final dispersion of Fe_3O_4.OA nanoparticles in toluene resulted in a highly stable ferrofluid having the prescribed concentration of individual MNPs (approx.0.10 solid volume fraction), to be used in the synthesis of magnetic nanoparticle clusters. The batch-type procedure proved to be highly reproducible and provided approx. 60 grams/batch of hydrophobic Fe3O4.OA nanoparticles ready to be dispersed in toluene.

Following the basic procedure described in [25], the magnetic nanoparticle clusters were prepared by oil-in-water miniemulsion method in which the oil phase-the previously obtained ferrofluid- was dispersed in the aqueous phase, forming organic droplets in the aqueous medium. The toluene-based ferrofluid (FF) was added to the aqueous phase containing the surfactant SLS or CTAB (0.09 M) and the mixture was treated ultrasonically for 2 minutes to obtain small stable droplets of magnetic nanofluid in water. The as prepared miniemulsion was then heated at 100° C to remove the toluene and then carefully washed several times with a methanol-water mixture, magnetically separated and redispersed in water. The

synthesis procedure of NPCs coated with the surfactants SLS or CTAB is highly reproducible and is suitable for up-scaling. The hydrophilic NPCs were further used for encapsulation into polymers.

Preparation of magnetic microgels

The CEX magnetic microgels were obtained by coating the NPCs stabilized with SLS either with one polymer shell of polyacrylic acid (pAAc) - sample *M1-pAAc*, or with two polymer shells using layer by layer free radical polymerization of poly-N-isopropylacrylamide (pNIPA) and pAAc, respectively – sample *M2-pNIPA-pAAc* [25]. The organic part of the magnetic microgels ensures biocompatibility, while the functional groups of polymers allow the specific binding of certain types of biomolecules [26]. In a three-neck flask 100 mL of aqueous solution containing NPCs, the monomer and the crosslinking agent BIS was stirred magnetically for 10 minutes under argon and then the oxidizing agent, APS has been added drop by drop. The reaction mixture was allowed to polymerize under magnetic stirring (600 rpm) in an oil bath at 70° C for 20 minutes, then the as formed microgels were precipitated using acetone (50 mL), followed by several times washing with water to remove unreacted compounds (3 x 50 mL) and finally redispersed in water (10 mL). The synthesis of the second layer, the polyacrylic acid, was performed by free radical polymerization of AAc in aqueous solution containing the NPCs coated with pNIPA, the crosslinker BIS and the oxidant APS using the same polymerization conditions.

The AEX magnetic microgels were prepared using the free radical polymerization of the APTAC monomer in aqueous solution in the presence of the NPCs covered with CTAB, the crosslinking agent BIS, a reaction accelerator TMEDA and the oxidizer APS. For the preparation of the AEX microgels the same polymerization conditions like in the case of CEX microgels are used. The as-prepared AEX microgel – sample *M3-pAPTAC* – was subjected to the precipitation and washing routine described above.

Characterization

The morphology of the magnetic nanoparticle clusters and magnetic microgels was investigated by transmission electron microscopy (TEM) using a TECNAI F30 G2 S-TWIN microscope operated at 300 kV. Samples derived from aqueous suspensions were dried on a double copper grid (oyster) prior to TEM analysis.

The surface chemical composition of magnetic nanoparticle clusters and magnetic microgels was investigated by X-ray Photoelectron Spectroscopy (XPS) using a XPS spectrometer SPECS equipped with a dual-anode X-ray source Al/Mg, a PHOIBOS 150 2D CCD hemispherical energy analyzer and a multi-channeltron detector with vacuum maintained at 1 x 10^{-9} torr. The Al$_{K\alpha}$ X-ray source (1486.6 eV) operated at 200W was used for XPS investigations. The XPS survey spectra were recorded at 30 eV pass energy, 0.5 eV/step. The high resolution spectra for individual elements were recorded by accumulating multiple scans at 30 eV pass energy and 0.1 eV/step. The particle suspension was dried on an indium foil to allow the XPS measurements.

Data analysis and curve fitting was performed using CasaXPS software with a Gaussian-Lorentzian product function and a non-linear Shirley background substraction.

The static magnetization of the samples was measured by means of vibrating sample magnetometry (VSM) at room temperature using an *ADE Technologies VSM 880* magnetometer.

The magnetically induced phase condensation in aqueous dispersions of the *M1-pAAc*, *M2-pNIPA-pAAc* and *M3-pAPTAC* samples was investigated by: (i) optical microscopy (OM) using an *OPTIKA N-400LD* microscope equipped with a CCD camera and a magnetic field generator, and (ii) Static Light Scattering (SLS) using an in-house built optical bench [27, 28].

Magnetic separation experiments

Magnetic separation experiments of the microgels were used to compare their behaviour in practical application and to determine both stability and magnetization in a standard separation procedure. The High Gradient Magnetic Separator (HGMS) that was used [29] contains a water-cooled electromagnet for generation of the magnetic field (0.25 T) and a rotor-stator unit (25 stainless steel discs arranged in rotor-stator-pairs) for redispersion of particles. The chamber holds a total volume of 1L. A smaller version of such a separator has also been described recently in [30]. The applied flow rate resulted in a mean residence time of the liquid in the separation chamber of approximately 90s. The particle concentration in the feed stream was set to 10g/l (*M1-pAAc*) and 5g/l (*M2-pNIPA-pAAc*, *M3-pAPTAC*). Additionally, a concentration of 20mM sodium chloride was applied to the feed stream to simulate a biological buffer system.

The separation efficiency is defined as the mass of particles magnetically separated divided by the total particle mass entering the system. It is determined by concentration measurements of samples taken from the effluent stream and calculated by:

$$E = 1 - \frac{c_{outlet}}{c_{inlet}} \tag{1}$$

As an analytical tool for concentration measurement a turbidimeter was applied, using different dilutions of the original feed solution as a calibration. This technique offers the advantage of being simple, fast and provides the possibility of continuous online measurement. When using gravimetric determination, continuous measurement is inaccurate or impossible, especially for very low concentrations.

Dilutions of the original feed suspensions were prepared with a dilution factor of 1:100 and 1:1000 using a solution of 20 mM NaCl in demineralized water. These diluted samples were used as measurement standards and compared to the turbidity T of samples taken every 45 s at the outlet during the separation process. From this the separation efficiency was calculated to be:

$$E = \left(1 - \frac{T_{outlet}}{T_{dilution1:100} * 100}\right) * 100\% \tag{2}$$

or

$$E = \left(1 - \frac{T_{outlet}}{T_{dilution1:1000} * 1000}\right) * 100\% \tag{3}$$

respectively. The measurement standards are chosen according to the sample's turbidity: in the low range the 1:1000 dilutions were used, while for higher turbidities the 1:100 dilutions were applied.

3. Results and discussion

Morphology of magnetic microgels

A typical TEM image of the NPCs obtained by the oil- in- water miniemulsion method is shown in Fig. 1a. Oleic acid coated magnetite nanoparticles from the toluene based ferrofluid are closely packed into spherical clusters stabilized with the surfactant SLS, as can be seen in the high resolution TEM image from Fig.1c. This can be attributed to the dominance of isotropic van der Waals interactions over the anisotropic magnetic dipole-dipole ones [28], which are well screened by the OA coating of nanoparticles.

The size distribution of the magnetic nanoclusters shown in Fig. 1b was obtained from TEM images using the image analysis software ImageJ. The normalized distribution of diameters is well described by a log-normal distribution function:

$$f(D) = \frac{1}{D\sigma\sqrt{2\pi}} \exp\left[-\frac{1}{2}\left(\frac{\ln^2 D/D_0}{\sigma^2}\right)\right] \qquad (4)$$

where D is the diameter, D_0 is the median diameter and σ is the standard deviation of the diameter's natural logarithm.

The best fit of the histogram from Fig. 1b was obtained with the parameters: D_0=96.2 nm, σ =0.40.

The selected area electronic diffraction patterns measured on magnetic nanoparticle clusters is shown in Fig. 1d. All electron diffraction rings are assigned to the face centered cubic crystalline structure of the magnetite, in accordance with ICDD (International Center for Diffraction Data) file number 04-005-4404.

The NPCs stabilized with CTAB show a similar distribution of diameters as that one from the Fig. 1b and the best fit parameters with log-normal function are: D_0=95.9 nm, σ =0.33. TEM images of the magnetic microgels and their size distributions are given in Fig. 2. The fitting parameters with log-normal function for the size distributions of magnetic microgels samples are given in the Figs. 2b, 2f and 2k. A comparison of the size distributions shows the largest average size was obtained for the microgel particles in sample *M2-pNIPA-pAAc* as expected for a double layer polymer coated NPCs. HRTEM images of the microgel samples given in Figs. 2d, 2h, 2i, 2l and 2m evidence the core-shell structure of spherical shape microgel particles. The close-packed magnetite nanoparticles can be observed in the core and their crystalline planes can be seen in the Fig.2i. The thin amorphous polymeric shell (1.5-5nm thick) coating the magnetite nanoparticles cluster is clearly evidenced in the Figs. 2d, 2h, 2i, 2l and 2m.
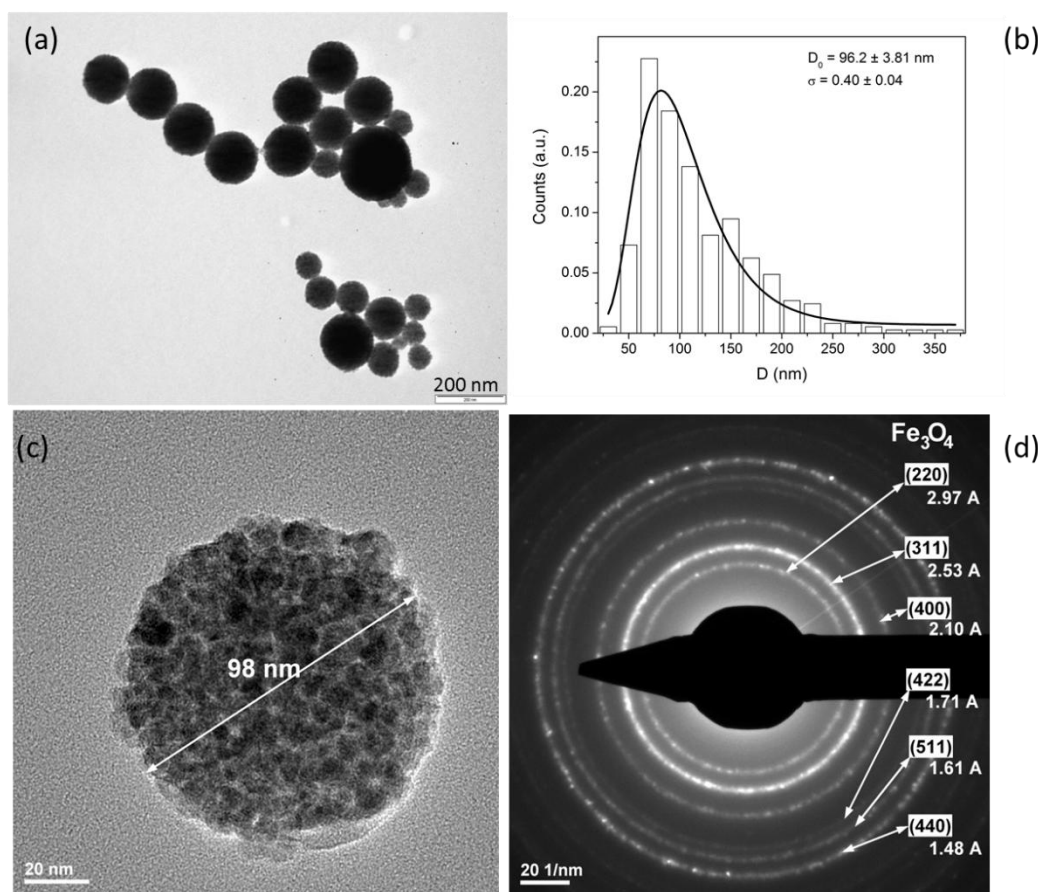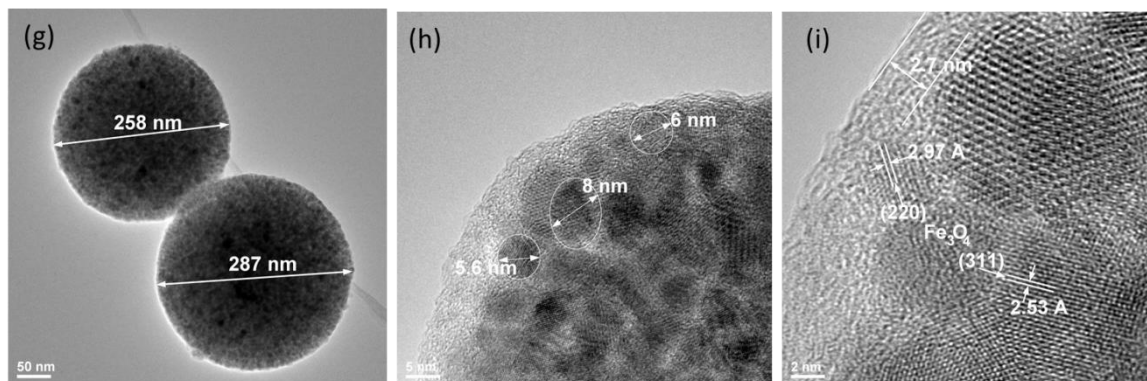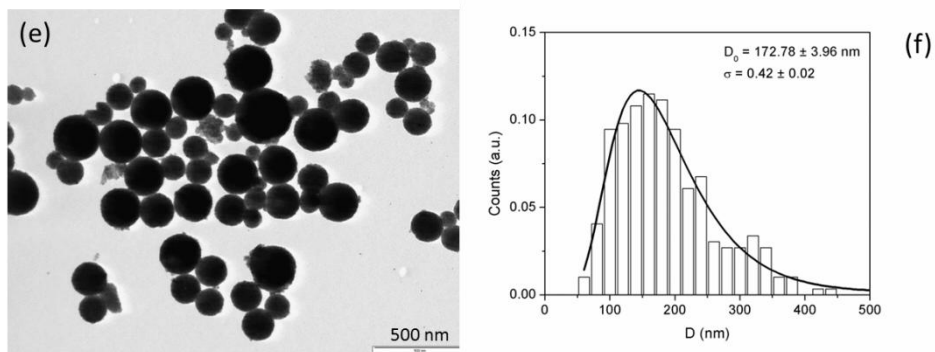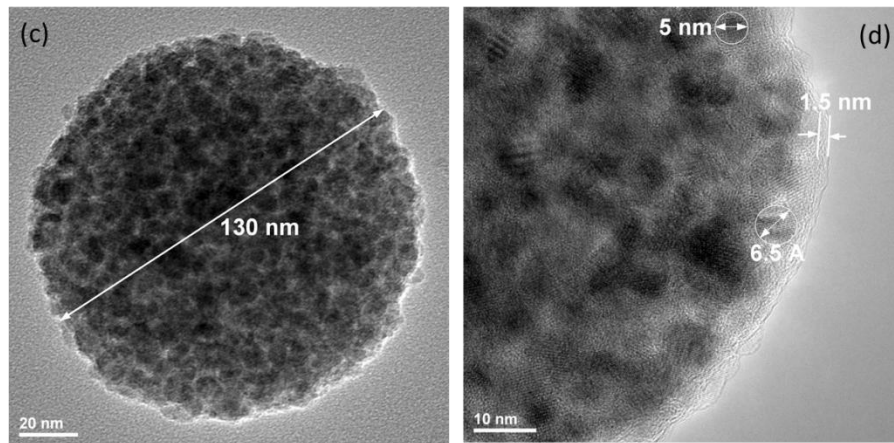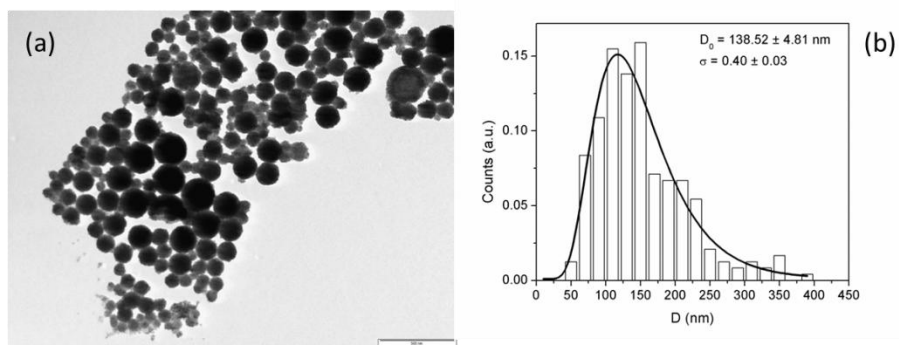

Fig. 1 Magnetic nanoparticle clusters stabilized with SLS: (a), (c) TEM images; (b) the diameter's distribution; (d) the electron diffraction pattern of the nanoparticle clusters.
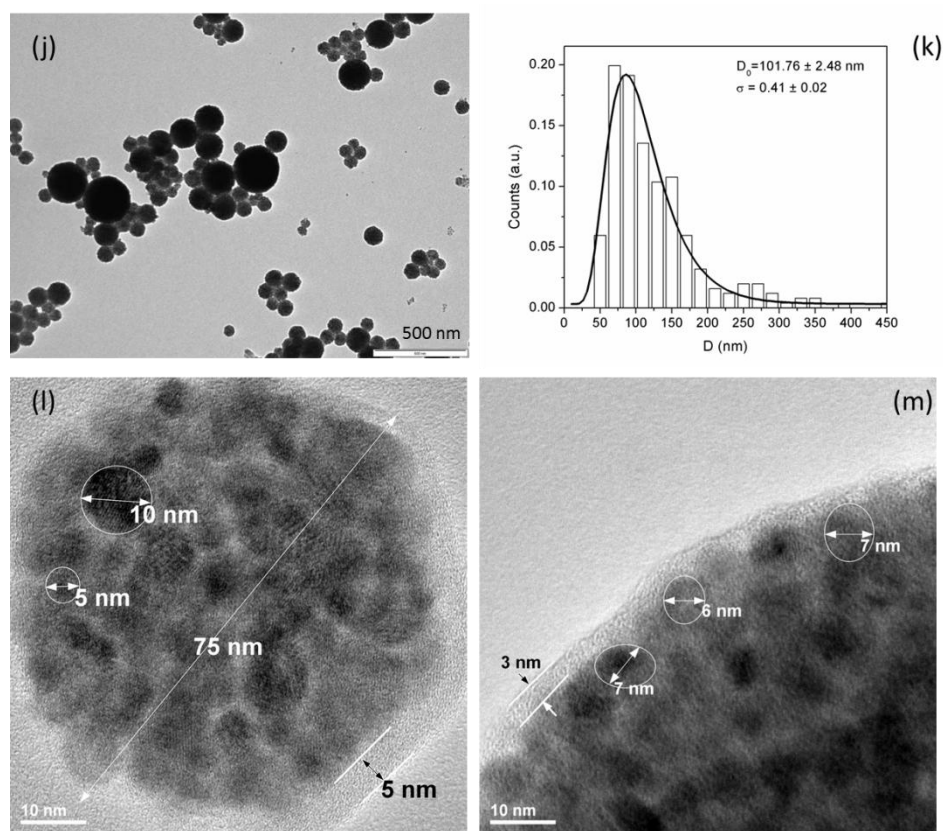
Fig. 2 TEM images of magnetic microgels and their size distributions: (a)-(d) sample *M1-pAAc*; (e)-(i) sample *M2-pNIPA-pAAc*; (j)-(m) sample *M3-pAPTAC*.

From the particle size distributions (Fig.2) of the produced microgels it can be seen that their average diameter is in the range of 100 to 200 nm. Therefore, even if a shape of smooth spheres would be assumed, the specific surface of the microgels clearly exceeds the value of 20 m²/g, the lower limit for the recommended specific surface area of magnetic adsorbents [10].

XPS analysis of magnetic microgels

XPS analysis was used to validate the successful coating of NPCs with polymers having carboxylic or ammonium groups. In Fig. 3 the high resolution XPS spectra of C1s, O1s, N1s, S2p and Fe2p core-levels of the CEX magnetic microgel sample *M2-pNIPA-pAAc*, obtained by coating the NPCs stabilized with SLS with a double layer of polymers poly(N-isopropylacrylamide) and polyacrylic acid, is given. The best fit for C1s spectrum was obtained with four components: the most intense component located at 285.25 eV corresponds to C-C, C-H; the components at 286.12 eV and 287.8 eV correspond to C-N and to the amide group N-C=O, respectively, from pNIPA and from the crosslinker BIS; the higher binding energy component located at 288.9 eV correspond to O-C=O group from pAAc [32]. The oxygen spectrum in Fig. 3 exhibits three components assigned to the oxygen atoms from carboxyl group -O–C=O of p-AAc (532.49 eV), from C=O, OSO$_3$ (530.65 eV)

and from Fe-O in magnetite, In-O sample support (528.97 eV), respectively. The N1s core-level spectrum from Fig. 3 shows one peak ascribed to the amine group –NH- from pNIPA. The coating of NPCs with the surfactant SLS is evidenced by the intense band located at 530.65 eV ascribed to OSO$_3$ group in the O1s spectrum (Fig. 3) and also by the S2p spectrum containing the doublet S2p3/2 and S2p1/2 at binding energies 168.54 eV and 169.7 eV, respectively, which correspond to sulfur atoms from sulfate [33]. The Fe2p core-level spectrum contains the doublet Fe 2p3/2 and Fe 2p1/2, but the low intensity of these peaks makes their deconvolution difficult. The fitting parameters including the peak positions, full width at half maximum (FWHM) and calculated atomic concentrations from peak areas for the sample M2-pNIPA-pAAc are given in Table 1.

The high resolution XPS spectra of C1s, O1s, N1s, Cl2p and Fe2p core-levels from AEX magnetic microgel sample *M3-pAPTAC*, obtained by coating the NPCs stabilized with CTAB with pAPTAC, are shown in Fig. 4. The deconvolution of C1s, O1s and N1s spectra and also the characteristic peak for Cl2p in Fig. 4 provide evidence of the polymer pAPTAC coating of NPCs. C1s contains three components ascribed to C-C, CH (284.68 eV), C-N (285.86 eV) and N-C=O (287.87 eV). The best fit of O1s spectrum was obtain with two components corresponding to oxygen atoms from the Fe-O, In-O support (529.23 eV) and C=O (531.2 eV). The N1s spectrum from Fig.

4 exhibits two components assigned to the nitrogen from the amine group –NH- and to positively charged nitrogen from pAPTAC. The higher intensity of Fe2p peaks for sample *M3-pAPTAC* from Fig. 4 in comparison with the one from Fig. 3 evidences a thinner pAPTAC shell than the pNIPA-pAAC coating NPCs in agreement with the results for the average diameters determined by TEM analysis (Fig. 2 b) and c)). The Fe 2p spectrum contains the doublet Fe 2p3/2 and Fe 2p1/2. The contribution from the indium support can be observed at low energies 700-705 eV. The best fit for the Fe2p spectrum in Fig. 4 contains the components corresponding to Fe^{3+} and Fe^{2+} ions and their corresponding satellites. [34, 35]. The fitting parameters of the XPS spectra for the sample *M3-pAPTAC* are given in Table 2.

Table 1: Fitting parameters of XPS spectra (Fig. 3) for the sample *M2-pNIPA-pAAc*

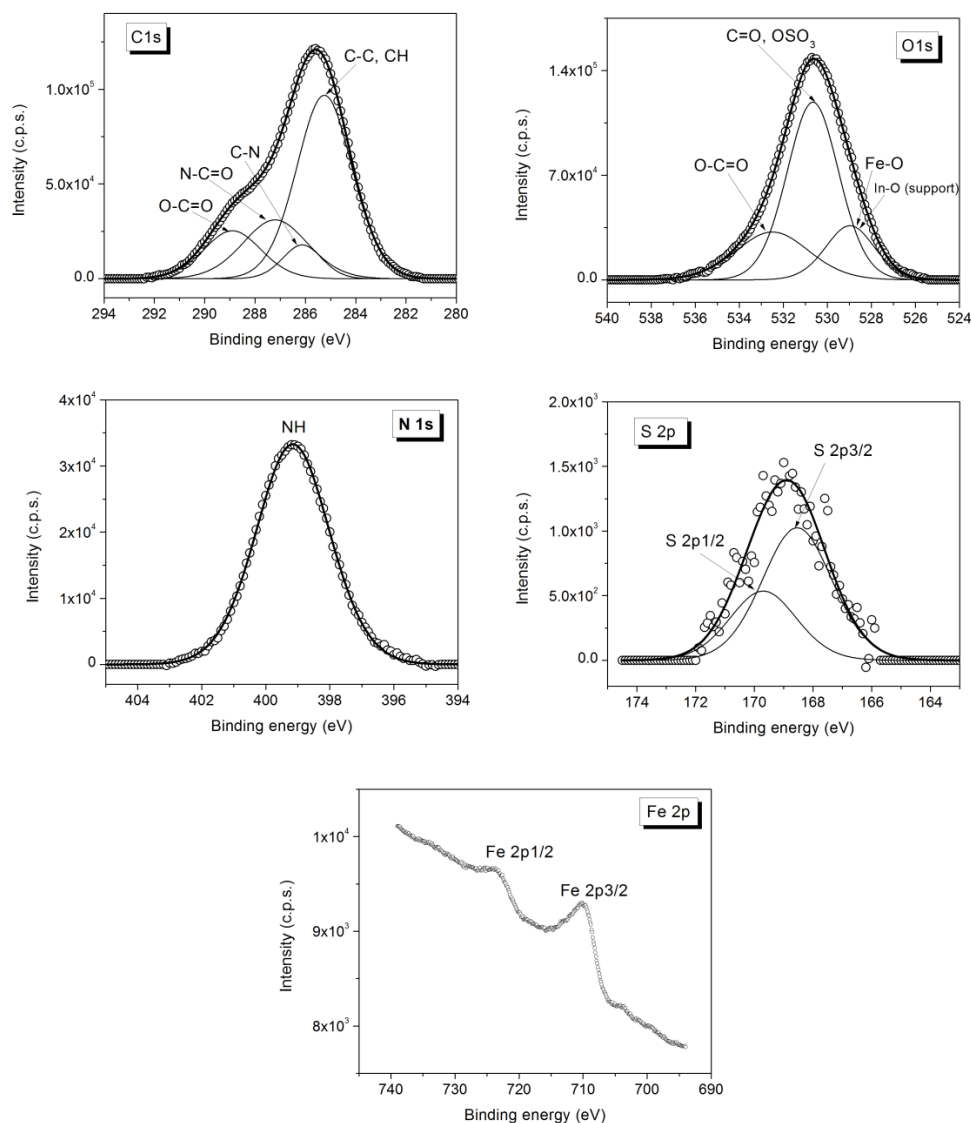| Peak name	Position (eV)	FWHM (eV)	% atomic concentration
C 1s	285.25	2.601	37.756
C 1s	286.12	1.835	4.922
C 1s	287.80	3.031	14.117
C 1s	288.90	2.692	10.237
O 1s	528.97	2.609	4.312
O 1s	530.65	2.776	15.039
O 1s	532.49	3.908	5.695
N 1s	399.16	2.700	7.118
S 2p3/2	168.54	2.809	0.407
S 2p1/2	169.70	2.688	0.398

Fig. 3 High resolution XPS spectra of C1s, O1s, N1s, S2p, Fe2p core levels from magnetic microgel sample *M2-pNIPA-pAAc*.
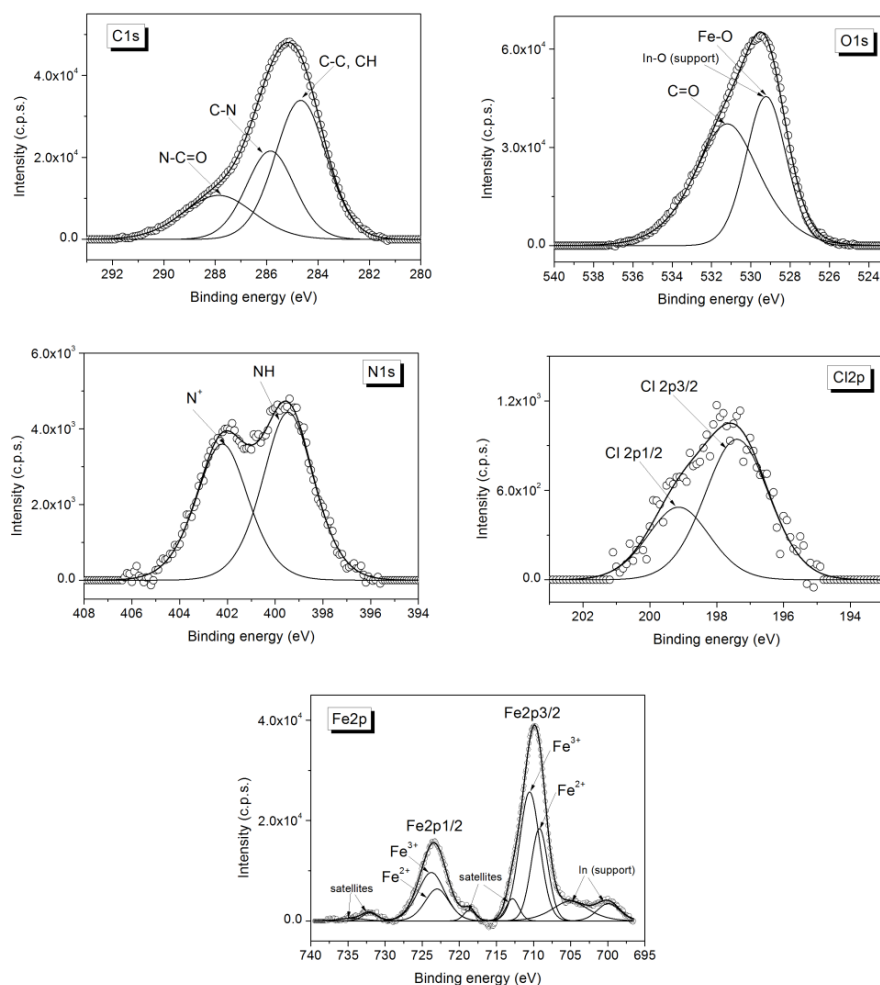
Fig. 4 High resolution XPS spectra of C1s, O1s, N1s, Cl2p and Fe2p core levels from magnetic microgel sample *M3-pAPTAC*.

Table 2: Fitting parameters of XPS spectra (Fig. 4) for the sample *M3-pAPTAC*

Peak name	Position (eV)	FWHM (eV)	% atomic concentration
C 1s	284.68	2.350	26.565
C 1s	285.86	2.215	15.923
C 1s	287.87	3.245	11.619
O 1s	529.23	2.407	13.160
O 1s	531.20	3.870	18.018
N 1s	399.45	2.526	2.179
N 1s	402.22	2.581	1.806
Fe^{2+} 2p3/2	709.21	2.698	1.700
Fe^{3+} 2p3/2	710.54	3.240	2.854
Fe 2p3/2 satellite	712.85	2.080	0.317
Fe 2p3/2 satellite	718.64	1.852	0.137
Fe^{2+} 2p1/2	723.00	3.853	1.646
Fe^{3+} 2p1/2	723.78	4.263	2.763
Fe 2p1/2 satellite	732.00	2.408	0.258
Fe 2p1/2 satellite	734.40	4.103	0.142

Magnetic properties of magnetic microgels

The magnetization curves of NPCs and magnetic microgel samples at room temperature (Fig. 5 and 6) show superparamagnetic behaviour, as it is expected for magnetite nanoparticles of small sizes (less than 10 nm) which are stabilized by oleic acid. Moreover, this fact indicates that the magnetite nanoparticles are still well separated after cluster formation.

The saturation magnetization M_S of NPCs has relatively high values: M_S=63.9 A·m^2/kg for NPCs stabilized with SLS; M_S=76.7 A·m^2/kg for NPCs stabilized with CTAB.

After polymer coating of NPCs stabilized with SLS and CTAB, the magnetization of the microgels decrease: M_S=46.8 A·m^2/kg for *M1-pAAc*; M_S=43 A·m^2/kg for *M2-pNIPA-pAAc*; M_S=55 A·m^2/kg for *M3-pAPTAC*. These high magnetization values ensure a high magnetic moment for each particle so that even small microgel particles are separated, resulting in a magnetic separation efficiency of above 99.9% (Fig.10).
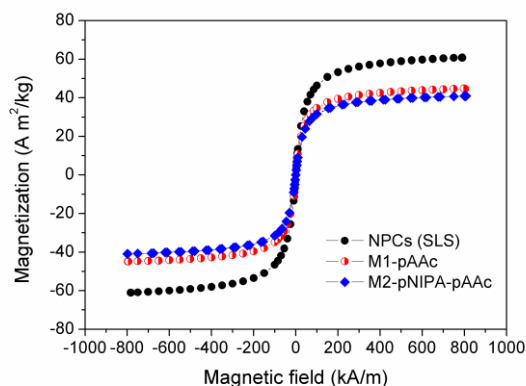
Fig. 5 Magnetization curves at room temperature of NPCs stabilized with SLS and of magnetic microgels obtained by coating the NPCs with polymers, samples *M1-pAAc* and *M2-pNIPA-pAAc*.
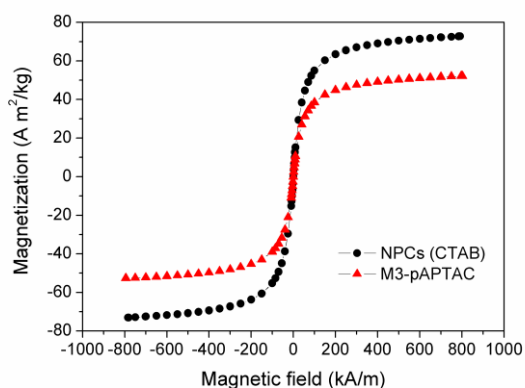

Fig. 6. Magnetization curves at room temperature of NPCs stabilized with CTAB and of magnetic microgels obtained by coating the NPCs with polymer, sample *M3-pAPTAC*.

Magnetically induced phase condensation in aqueous dispersions of magnetic microgels

The magnetically induced phase condensation [36-38] leads to the formation of oblong condensed phase drops (CPDs) of highly packed magnetic colloidal particles. The condensed phase is in equilibrium with the depleted aqueous dispersion of magnetic colloidal particles. The condensed phase drops are aligned parallel to the external magnetic field and may grow up to several microns thickness and tens or even hundreds of microns length [27, 28].

The influence of the magnetic field on the structure of aqueous dispersions of the three types of microgels (*M1-pAAc*, *M2-pNIPA-pAAc* and *M3-pAPTAC*) was investigated. The microgel volume fractions in the aqueous dispersions were the same as those used in the magnetic separation experiments. Only the *M3-pAPTAC* sample showed magnetically induced phase condensation.

The magnetically induced phase condensation in sample *M3-pAPTAC* was investigated by optical microscopy at room temperature (25°C), in 16 kA/m magnetic field oriented parallel to the plane of an optical cell of 0.1 mm thickness, which contained the sample A few seconds after the sudden onset of the magnetic field, short but thick (~3 x 25 μm) drops of condensed phase start to form (Fig. 7 left). These primary CPDs are oriented in the field direction and move slowly in the cell. During the next minutes, the slow moving primary CPDs stick together head-to-tail to form very long (>200 μm) and almost motionless needle-like secondary CPDs (Figure 7 right). The secondary CPDs have the same thickness as the primary CPDs. After the magnetic field was turned off, the condensed phase drops dissolved almost instantaneously. The observed evolution of the condensation process is the same as both the theoretical picture of the magnetically induced phase condensation kinetics developed by Ivanov and Zubarev [39] for ferrofluids, and the experimental findings reported in the literature on various types of magnetic colloids [27, 40-42].

The kinetics of the magnetically induced phase condensation in sample *M3-pAPTAC* was investigated by means of Static Light Scattering. For details about the experiment, theory and data processing see ref. [28]. In a nut shell, the forward scattered light decreases with growing weight of the condensed phase drops.

In Fig. 8 the time evolution of the forward scattered light intensity $I(t)/I(t=0)$ at 25°C is presented, for four values of the magnetic field intensity: 8, 40, 80, 160 kA/m. The field was switched on at t=0 s and when the phase condensation reached equilibrium it was switched off, waiting for the condensed phase drops to dissolve. Each measurement was made on a fresh sample, i.e. not previously exposed to an external magnetic field. The initial sudden increase of the forward scattered light intensity is due to sample dichroism (light was polarized perpendicular to the magnetic field direction) caused by the microgel clustering in linear chains. The subsequent slow decrease of the forward scattered light intensity is caused by the formation of the condensed phase drops. The decay rate of the forward scattered light intensity increases with increasing magnetic field, due to the enhanced magnetic dipole-dipole attraction among the microgels. After the field was switched off, the dissolution of the CPDs occurs in a matter of seconds. In the inset of Fig. 8 the temperature influence on the time evolution of the forward scattered light intensity is shown. There seems to be no significant influence of the increasing temperature on the magnetically induced phase condensation in the sample.

Using the total decay of the forward scattered light intensity, the magnetic field dependence of the weight of microgels contained in the CPDs (i.e. the magnetic supersaturation) was calculated with the methodology developed in ref. [28]. As one can see from Fig. 9, the magnitude of the magnetically induced phase condensation increases with the field intensity. In a 160 kA/m magnetic field, almost 80% of the microgels are entrapped in the CPDs.
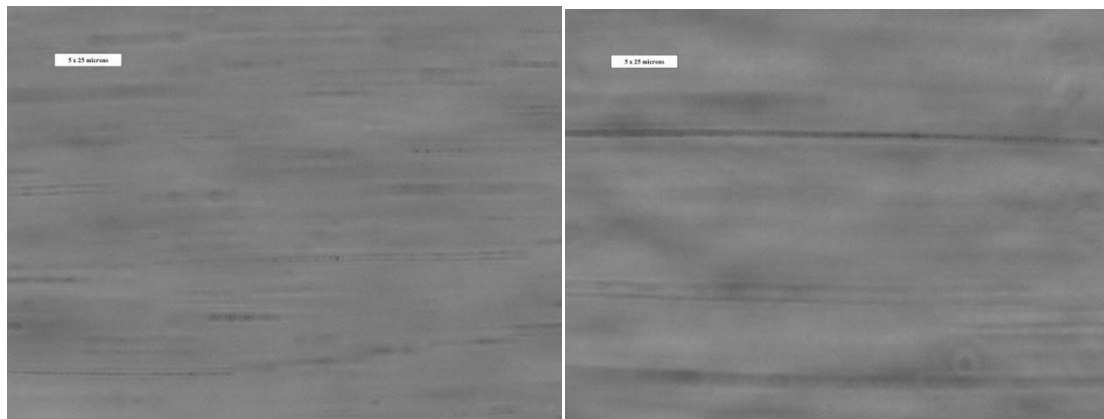
Soft Matter Accepted Manuscript

Fig. 7 Optical microscopy images of the condensed phase drops in the sample *M3-pAPTAC* after the onset of a 16 kA/m magnetic field: 30 sec. (left) and 5 min. (right). The bar is 5 x 25 μm.
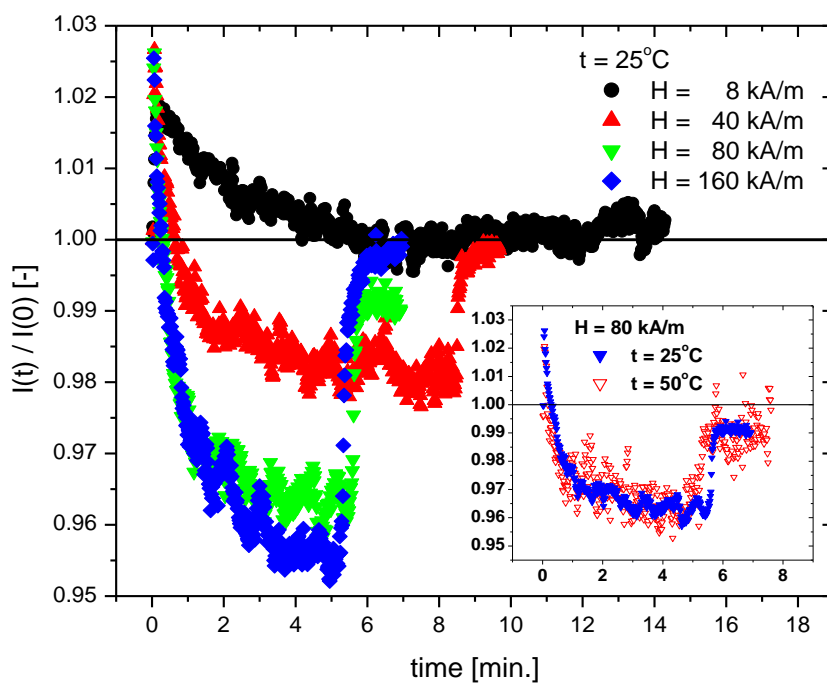

Fig. 8 The time evolution of the forward scattered light intensity by sample *M3-pAPTAC* at 25°C, for four values of the magnetic field intensity. The inset shows the temperature influence on the condensation behavior for a magnetic field intensity of 80 kA/m.
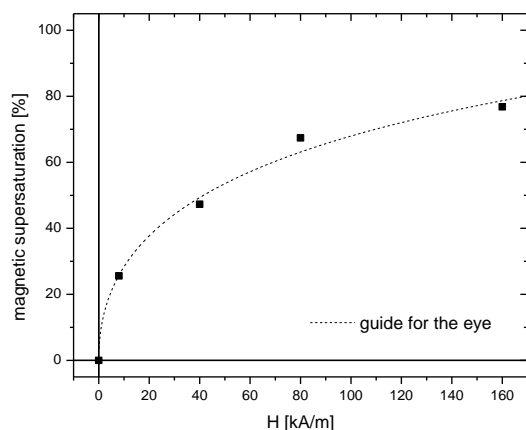
Fig. 9 The field dependence of the magnetic supersaturation for the sample *M3-pAPTAC*.

Separation efficiency of magnetic microgels

The separation efficiencies of the magnetic microgels are shown in Fig. 10. The separation efficiency is plotted versus the treated feed suspension volume.

As can be seen, the separation efficiency for the samples *M1-pAAc* and *M2-pNIPA-pAAc* stayed above 99.97% during the experiment. The microgel M3-pAPTAC had a slightly smaller separation efficiency of 99.9%, possibly due to the larger amount of small particles than the other two samples (see TEM images in Fig.2). For all separation efficiency curves a decrease is visible after about one liter of suspension volume has passed through the separator. This volume is equivalent to the dead volume of the device and therefore means that particles that are not separated in the field can be expected in the outlet only after this volume has passed.
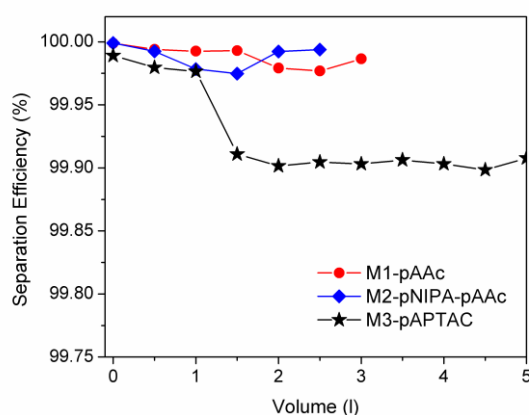

Fig. 10 Separation efficiency of the microgels plotted versus the treated suspension volume, particle concentration 5g/l (except *M1-pAAc*: 10 g/l), 20mM sodium chloride, 90s residence time in the magnetic field (0.25T).

High separation efficiencies were achieved, because even the small microgel particles were easily separated due to high magnetization of the investigated samples. For large scale applications of magnetic adsorbents, e.g. in the field of protein purification, a uniform particle size isn't required. As illustrated in fig.7, the particles quickly form temporary aggregates under the influence of a strong magnetic field (like in the separator) and uniformity does not offer clear advantages. The decisive property is the separation efficiency of the particle collective, which has to be above 99% for the process to be economic. Therefore, as can be seen in Fig.10, the microgels are well suited for tasks as protein purification or enzyme immobilization [26].

This result allows avoiding supplementary preparation steps for large scale manufacturing of microgel particles for magnetic bioseparation purposes.

4. Conclusions

High magnetization magnetic microgels have been obtained by using a toluene based magnetic nanofluid as a primary material in a two-step synthesis procedure: in a first step, well defined spherical clusters of closely packed hydrophobic oleic acid coated Fe_3O_4 nanoparticles were prepared using a miniemulsion method; in the second step these clusters were coated with cross-linked polymer shells of pAAc, pNIPA-pAAc, pAPTAC. The spherical shape microgel particles have a core-shell structure, as evidenced by HRTEM. The thickness of the amorphous polymeric shell coating the magnetic core of close packed magnetic nanoparticles is in the range of 1.5-5nm. The high resolution XPS spectra evidence the composition details of the coating of magnetic clusters with polymer shells and validate the presence of functional groups with cation exchange or anion exchange properties. The magnetization curves of the magnetic microgels showed no measurable hysteresis or coercivity, consistent with the superparamagnetic behavior of these composite particles. The magnetically induced phase condensation was observed only for AEX magnetic microgel *M3-pAPTAC*. The condensed phase consists of elongated oblong structures oriented in the direction of the external magnetic field. The magnetically induced phase condensation has no influence on the separation efficiency of AEX microgel which is 99.9 % as compared with that one for CEX microgels which is above 99.97%. The high values of the separation efficiency for the magnetic microgels demonstrate their applicability for magnetic separation of biomaterials. The high reproducibility of the carefully designed procedure for the synthesis of magnetic microgels allowed the preparation of hundreds grams of microgel particles for magnetic separation experiments, keeping an adequate balance of the preparation costs and the application orientated requirements.

Notes and references

[a] National Institute R&D for Isotopic and Molecular Technologies, 67-103 Donat Str., RO-400293 Cluj-Napoca, Romania.

[b] Romanian Academy-Timisoara Branch, Center for Fundamental and Advanced Technical Research, Lab. Magnetic Fluids, 24 M. Viteazu Ave., RO-300223 Timisoara, Romania.

[c] Karlsruhe Institute of Technology (KIT) Institute of Functional Interfaces, Hermann-von-Helmholtz-Platz 1, 76344 Eggenstein-Leopoldshafen, Germany.

[d] University Politehnica of Bucharest, Faculty of Applied Chemistry and Material Science, Department of Oxide Materials and Nanomaterials, 1-7 Gh. Polizu Street, 011061 Bucharest, Romania

[*] **Corresponding authors:**

Rodica Turcu, E-mail: rodica.turcu@itim-cj.ro

Vlad Socoliuc, E-mail: vsocoliuc@gmail.com

Ladislau Vekas, E-mail: vekas.ladislau@gmail.com

1. A.M. Schmidt, *Colloid Polym. Sci.* 2007, **285**, 953.
2. J. Kim, J.E. Lee, S.H. Lee, J.H. Yu, J.H. Lee, T.G. Park, T. Hyeon, *Adv. Mater*. 2008, **20**, 478.
3. J.K. Oh, J.M. Park, *Prog. Polym. Sci.,* 2011, **36**, 168.
4. E. Amstad, M. Textor, E. Reimhult, *Nanoscale*, 2011, **3,** 2819.
5. L. Borlido, A.M.Azevedo, A.C.A. Roque, M.R. Aires-Barros, Biotechnology Advances, 2013, **31**, 1374
6. K. Mosbach, L. Anderson, *Nature*, 1977, **270**, 259.
7. T. Griffin, K. Mosbach, R. Mosbach, *Applied Biochemistry and Biotechnolog*y, 1981, **6**, 283.
8. J. Ugelstad, L. Soderberg, A. Berge, J. Bergström, *Nature*, 1983, **303**, 95.
9. A. Meyer, D.B. Hansen, C.S. Gomes, T.J. Hobley, O.R. Thomas, M. Franzreb, *Biotechnol. Progr*., 2005, **21**, 244.
10. M. Franzreb, M. Siemann-Herzberg, T.J. Hobley, O.R. Thomas, *Appl. Microbiol. Biotechnol*., 2006, **70**, 505.
11. J. Muzard, M. Platt, G.U. Lee, *Small*, 2012, **8**(15), 2403.
12. H. Nirschl, K. Keller (Eds), Upscaling of bio-nano-processes, Springer (2014) 245p.
13. A. Dietsch, P.E. Laibinis, D.I.C. Wang, T.A. Hatton, *Langmuir,* 2005, **21**, 6006.
14. H. Chang, W.-S. Chang, S. Kan, S.A. Majetich, G.U. Lee, *Langmuir*, 2006, **22**, 2516.
15. M. Laurenti, P. Guardia, R. Contreras-Caceres, J. Perez-Juste, A. Fernandez-Barbero, E. Lopez-Cabarcos, J. Rubio-Retama, *Langmuir*, 2011, **27**, 10484.
16. J.J. O'Mahony, M. Platt, D. Kilinc, G. Lee, *Langmuir*, 2013, **29**, 2546.
17. P. Qiu, C. Jensen, N. Charity, R. Towner, C. Mao, *J. Am. Chem. Soc*., 2010, **132**, 17724.
18. M.S.A. Darwish, U. Peuker, U. Kunz, T. Turek, *J. Mater. Sci*., 2011, **46**, 2123.
19. M.S.A. Darwish, S.Machunsky, U.Peuker, U. Kunz, T.Turek, *J. Polym. Res*. 2011, **18**, 79.
20. V. Lobaz, R. N. Klupp Taylor, W. Peukert, *J. Coll. Interface Sci*., 2012, **374**, 102.
21. C. Kaewsaneha, P. Tangboriboonrat, D. Palpanich, M. Eissa, A. Elaissari, *J. Coll. Interface Sci*., 2013, **409**, 66.
22. B. Luo, X.J. Song, F. Zhang, A. Xia, W. L. Yang, J.H. Hu, C. C. Wang, *Langmuir*, 2010, **26**, 1674.
23. K. Landfester*, Annu. Rev. Mater. Res*., 2006, **36**, 231.
24. V. Socoliuc, L. Vekas, in: H. Nirschl, K. Keller (Eds), Upscaling of bio-nano-processes, Springer (2014) pp.39-56
25. R. Turcu, I. Craciunescu, A. Nan in: H. Nirschl, K. Keller (Eds), Upscaling of bio-nano-processes, Springer (2014) pp.57-76
26. A. Paulus, M. Franzreb, in: H. Nirschl, K. Keller (Eds), Upscaling of bio-nano-processes, Springer (2014) pp.175-186
27. V. Socoliuc, D. Bica*, Progress in Colloids and Polymer Science*, 2002, **117,** 131.
28. V. Socoliuc, L. Vekas, R. Turcu, *Soft Matter,* 2013*,* **9**, 3098.
29. M. Franzreb, C. Reichert, 2009. High Gradient Magnetic Separator. United States Patent. Patent No.: US 7506765 B2
30. G. N. Brown, C. Müller, E. Theodosiou, M. Franzreb, O.R.T. Thomas, *Biotechnology and Bioengineering*, 2013, **110**(6), 1714.
31. Y. Lalatonne, J. Richardi, M. Pileni, *Nature Materials*, 2004, **3**, 121.
32. G. Beamson, D. Briggs, *High resolution XPS of Organic Polymers*; *The Scienta ESCA300 Database*; John Wiley and Sons, Ltd.: Chichester, England, 1992.
33. B. J. Lindberg, K. Hamrin, G. Johansson, U. Gelius, A. Fahlman, C. Nordling, K. Siegbahn, *Phys Scr*., 1970, **1,** 286.
34. M. Descostes, F. Mercier, N. Thromat, C. Beaucaire, M. Gautier-Soyer, *Appl. Surf. Sci*., 2000, **165**, 288.
35. G. Bhargava, I. Gouzman, C.M. Chun, T.A. Ramanarayanan, S.L. Bernasek, *Appl. Surf. Sci*., 2007, **253,** 4322.

ARTICLE

36. J.C. Bacri, D. Salin, *J. Magn. Magn. Mater.,* 1983, **39**, 48.

37. A. Cebers, *J. Magn. Magn. Mater.,* 1990, **85**, 20.

38. Yu. A. Buyevich, A.O. Ivanov, *Physica A*, 1992, **190**, 276.

39. A.Yu. Zubarev, A.O. Ivanov, *Phys. Rev. E* , 1997, **55**, 7192.

40. J. C. Bacri, D. Salin, *J. Physique – LETTRES,* 1982, **43**, L-649.

41. M. T. López- López, A. Yu. Zubarev, G. Bossis, *Soft Matter,* 2010, **6**, 4346.

42. C. Magnet, P. Kuzhir, G. Bossis, A. Meunier, S. Nave, A. Zubarev, C. Lomenech, and V. Bashtovoi, *Phys. Rev. E* , 2014, **89**, 032310.
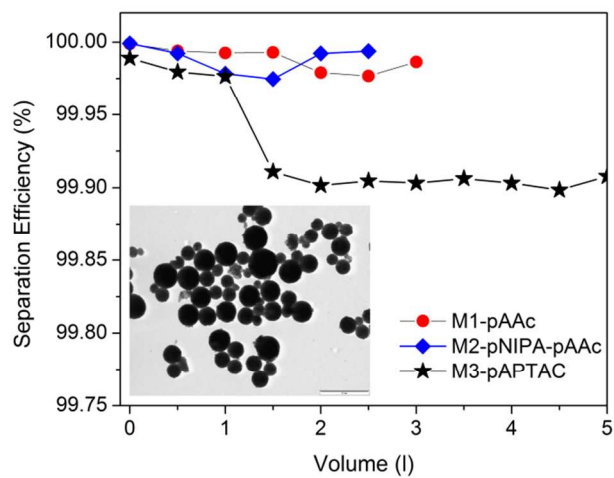
High magnetization spherically shaped superparamagnetic functionalized microgels of 100-200 nm with 99.9% separation efficiency synthesized by ferrofluid based miniemulsion procedure